



Title	Decomposition and determination of thermal conductivity of MOFs with fluid molecules via equilibrium molecular dynamics
Author(s)	Ito, Hideaki; Fujiwara, Kunio; Shibahara, Masahiko
Citation	International Journal of Heat and Mass Transfer. 2024, 228, p. 125676
Version Type	VoR
URL	https://hdl.handle.net/11094/97170
rights	This article is licensed under a Creative Commons Attribution 4.0 International License.
Note	

The University of Osaka Institutional Knowledge Archive : OUKA

<https://ir.library.osaka-u.ac.jp/>

The University of Osaka



Decomposition and determination of thermal conductivity of MOFs with fluid molecules via equilibrium molecular dynamics

Hideaki Ito^{*}, Kunio Fujiwara, Masahiko Shibahara

Department of Mechanical Engineering, Graduate School of Engineering, Osaka University, 2-1 Yamadaoka, Suita, Osaka 565-0871, Japan

ARTICLE INFO

Keywords:

MOFs
Molecular dynamics
Heat transfer
Thermal conductivity

ABSTRACT

Metal-organic frameworks (MOFs) are promising porous materials for various applications, which have attracted considerable attention recently. Optimizing their thermal properties, such as their heat accumulation characteristics during the adsorption of fluid molecules, is crucial for enhancing their performance. Molecular dynamics studies are vital for meticulously understanding the thermal transport of MOFs. To determine the thermal conductivity of MOFs using the Green–Kubo formula through equilibrium molecular dynamics (EMD), the heat current autocorrelation function (HCACF) must be truncated at a specific time. However, few studies have been conducted on establishing a method for truncating HCACFs for MOFs, rendering it challenging to assess the reliability of MOF thermal conductivities calculated through EMD. In addition, previous studies focused on the overall thermal conductivity, and the contribution of the components have not been identified. In this study, we devised a method for determining the truncation time of an HCACF to calculate the thermal conductivity of MOFs. After confirming the validity of the method, we decomposed the instantaneous heat flux into individual components and obtained the decomposed thermal conductivities. The results revealed that the contribution of the interaction of atoms was more pronounced than that of the microscopic convection of atoms. In addition, the method introduces an ambiguity while calculating the thermal conductivity of MOFs through EMD. The proposed method is useful for truncating of HCACFs and determining the thermal conductivity of complex materials such as MOFs.

1. Introduction

Metal-organic frameworks (MOFs) are unique porous materials characterized by structures wherein metal clusters are connected by organic linkers. Their high surface area and porosity facilitate an excellent adsorption performance, and they hold considerable potential for various applications, such as gas storage [1–3], gas separation [4–10], sensing [11–13], and catalysis [14–18]. The combination of metal clusters and organic linkers can be tailored to produce MOFs with desired properties, allowing versatility in designing MOFs. In particular, MOFs have been developed as hydrogen [19,20] and carbon dioxide [21,22] adsorbents, which are expected to contribute to the mitigation of energy and environmental issues in the future. However, the adsorption capacity of MOFs may be reduced with increasing temperatures. Gas adsorption is an exothermic phenomenon. Therefore, heat accumulation due to rapid gas adsorption can affect the performance of MOFs.

To address this issue, it is crucial to understand the thermal-transport

properties of MOFs to design promising materials with efficient thermal transport. Among the tools available to study this issue, molecular simulation stands out as a powerful and widely used method for investigating the thermal-transport properties of materials at the molecular scale [23–30]. However, most studies using molecular simulations have focused on MOFs without fluid molecules, and study on MOFs incorporating fluid molecules is still limited, and an understanding of their thermal properties remains insufficient. In a previous study, the thermal conductivities of HKUST-1 loaded with water, methanol, and ethanol were investigated using equilibrium molecular dynamics (EMD) [28]. The results of the study revealed that fluid molecules have two effects on thermal conductivity: one is the decreasing effect by phonon scatterings; the other is the increasing effect by additional pathways of heat transport. The authors showed that the decreasing effect was dominant, which led to the reduction of the thermal conductivity. Another study examined the interface between HKUST-1 and water molecules and revealed that the thermal resistance at the interface is a bottleneck hindering the efficient dissipation of heat [27].

^{*} Corresponding author.

E-mail address: itou@mte.mech.eng.osaka-u.ac.jp (H. Ito).

<https://doi.org/10.1016/j.ijheatmasstransfer.2024.125676>

Received 29 December 2023; Received in revised form 30 March 2024; Accepted 5 May 2024

Available online 13 May 2024

0017-9310/© 2024 The Authors. Published by Elsevier Ltd. This is an open access article under the CC BY license (<http://creativecommons.org/licenses/by/4.0/>).

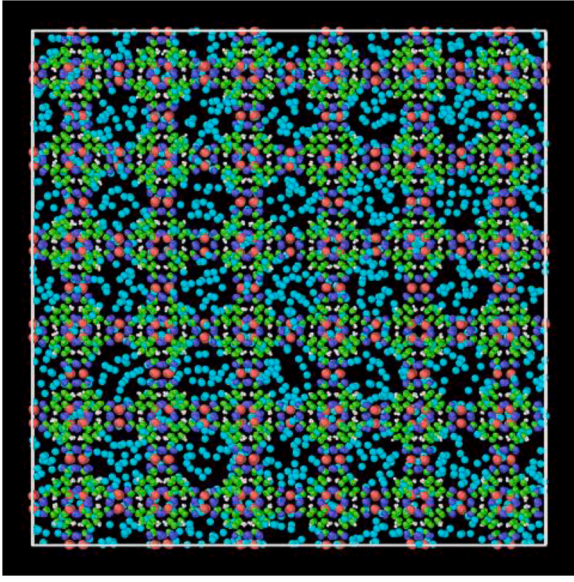


Fig. 1. Simulation system (Color coding: Cu; red, O; blue, C; green, H; white, Ar; cyan).

It is difficult to determine the thermal conductivity of materials using conventional EMD simulations. The heat current autocorrelation function (HCACF) should be integrated over infinite time when the thermal conductivity of the equilibrium system is calculated with the Green–Kubo formula [31,32]. However, the HCACF must be truncated at a certain correlation time in finite-time simulations. Moreover, thermal conductivities fluctuate over the integration time, impeding their accurate calculations. In previous studies, some researchers regarded the fluctuations of the HCACF observed over long correlation times as noise and determined the cutoff times [33] for the integration calculation. In this method, the cutoff time is defined as the correlation time when the noise exceeds the HCACF. In another method [34], a function is defined to quantify the relative fluctuations in the HCACF, and the cutoff time is determined using the magnitude of the function. However, the applicability of these methods to the systems composed of MOFs with or without fluids, has not been investigated.

Through previous studies, the decomposed thermal conductivities [35] of MOFs remain unclear. It is crucial to elucidate the contribution of each component of the heat flux to the thermal conductivity and the effect of fluid molecules on them for understanding the thermal-transport properties of MOFs.

In this study, we developed a method for determining the cutoff time for integrating the Green–Kubo formula and meticulously investigated the thermal transport of MOFs loaded with fluid molecules by decomposing the thermal conductivity. First, we investigated the applicability of the methods described in previous studies and then proposed an original method to truncate the HCACF in EMD simulations. After confirming the validity of the proposed method, we decomposed the thermal conductivity of HKUST-1 loaded with Ar atoms into each component of the instantaneous heat flux and investigated the relationship between the number of loaded Ar atoms and the thermal conductivities of the components, resulting in showing an ambiguity in the thermal conductivity calculation of MOFs by EMD simulations.

2. Computational details

HKUST-1 is a typical MOF consisting of Cu clusters and 1,3,5-benzenetricarboxylate ligands. We applied the force fields developed by Zhao et al. [36] for modeling the interactions between the atoms composing HKUST-1 and used a $3 \times 3 \times 3$ supercell. We chose Ar as the fluid molecule to eliminate the effects of shape, charge, and rotation of the

molecules on the results. The interactions between the atoms composing HKUST-1 and the Ar atoms were represented using the Lennard–Jones potential. The potential parameters for Ar were obtained using a universal force field (UFF) [37]. The initial configurations of the Ar atoms were determined using grand canonical Monte Carlo (GCMC) simulations. We generated six cases with different numbers of Ar atoms, 0 (pristine HKUST-1), 500, 1000, 1500, 2000, and 2500 atoms. The Ar atoms were then loaded into the HKUST-1 model. Fig. 1 shows an example of this system, wherein each side length is 7.98 nm. Periodic boundary conditions were applied in all directions. A Large-scale Atomic/Molecular Massively Parallel Simulator (LAMMPS) [38] was used for the simulation.

In this study, we used the Green–Kubo formula [31,32] to calculate the thermal conductivity of the MOF, as follows.

$$k = \frac{V}{3k_B T^2} \int_0^\infty \langle \mathbf{J}(t) \cdot \mathbf{J}(0) \rangle dt \quad (1)$$

In Eq. (1), $\mathbf{J}(t)$ is the instantaneous heat flux, V is the volume of the simulation system, k_B is the Boltzmann constant, and T is the temperature of the system. In addition, $\langle \mathbf{J}(t) \cdot \mathbf{J}(0) \rangle$ is the heat flux autocorrelation function, and $\mathbf{J}(t)$ was calculated by the Eq. (2) [39].

$$\mathbf{J}(t) = \frac{1}{V} \left[\sum_{j=1}^N \mathbf{v}_j E_j - \sum_{\alpha=1}^2 h_\alpha \sum_{j=1}^{N_\alpha} \mathbf{v}_{\alpha j} \right] + \frac{1}{V} \left[\frac{1}{2} \sum_{i=1}^N \sum_{j=1, j \neq i}^N \mathbf{r}_{ij} (\mathbf{v}_i \cdot \mathbf{F}_{ij}) \right] \quad (2)$$

Here, E_j is the instantaneous energy calculated as the sum of the kinetic and potential energies of atom j , and \mathbf{v}_j is the velocity of atom j . N and N_α are the number of atoms of the whole system and that of component α , respectively. \mathbf{r}_{ij} and \mathbf{F}_{ij} denote the displacement vector and interacting force between atoms i and j , respectively, and h_α is the average partial enthalpy of component α . h_α is not incorporated into the formula when calculating the instantaneous heat flux of the pristine HKUST-1. h_α was calculated as follows.

$$h_\alpha = \frac{\sum_{i=1}^{N_\alpha} \left[K_i + U_i + \frac{1}{3} \left(m_i v_i^2 + \frac{1}{2} \sum_{j=1}^{N_\alpha} \mathbf{r}_{ij} \cdot \mathbf{F}_{ij} \right) \right]}{N_\alpha} \quad (3)$$

Here, K_i and U_i are the time-averaged values of kinetic and potential energies of atoms, respectively, for the component α . On the right-hand side of Eq. (2), the first term represents the kinetic contribution with the microscopic convection of the atoms, and the second term is the contribution of the interactions between the atoms. Therefore, based on the previous study [39], the first term is called the “kinetic term” and the second term, the “virial term”. To validate the simulation, the thermal conductivity of pristine HKUST-1 was calculated using Eq. (2) under the same conditions as those employed in a previous study [26]. The thermal conductivity of pristine HKUST-1 was calculated to be 2.03 W/(m·K). In the previous study, the reported thermal conductivity of HKUST-1 was 1.65 W/(m·K), revealing an error of 23 % in our results. This error occurred because a correction for the calculation of the virial term was not applied in the previous study. When calculating the virial term, the virial stress tensor must be modified in accordance with the geometric center of the interacting atoms. In this study, a corrected stress tensor was used [40]. Without the correction, the thermal conductivity obtained was 1.73 W/(m·K), representing an error within 5 % compared to the value reported in the previous study.

The simulation was conducted as follows. First, the system temperature was maintained at 298 K for 500 ps. Then, an equilibration state was achieved in 100 ps. Finally, data were produced for 1 ns under NVE conditions. The time step was 0.5 fs and the HCACF was calculated every 5 ps with a correlation time of 50 ps. To obtain the thermal conductivity, the simulations were executed ten times with different initial velocities of the atoms, and an average value was subsequently obtained. We divided the kinetic terms $\left(\frac{1}{V} \left[\sum_{j=1}^N \mathbf{v}_j E_j \right] \right)$ and $\frac{1}{V} \left[\sum_{\alpha=1}^2 h_\alpha \sum_{j=1}^{N_\alpha} \mathbf{v}_{\alpha j} \right]$ of the

instantaneous heat flux (Eq. (2)) into the two terms: a term for HKUST-1 and that for Ar atoms. Only $J_{c1, \text{MOF}}$ and J_v are calculated for pristine HKUST-1, while J_v , $J_{c1, \text{MOF}}$, $J_{c1, \text{gas}}$, $J_{c2, \text{MOF}}$, and $J_{c2, \text{gas}}$ are calculated for Ar-loaded HKUST-1.

$$J_{c1, \text{MOF}} = \frac{1}{V} \left[\sum_{j=1}^{N_{\text{MOF}}} \mathbf{v}_j E_j \right] \quad (4)$$

$$J_{c1, \text{gas}} = \frac{1}{V} \left[\sum_{j=1}^{N_{\text{gas}}} \mathbf{v}_j E_j \right] \quad (5)$$

$$J_{c2, \text{MOF}} = \frac{1}{V} \left[h_{\text{MOF}} \sum_{j=1}^{N_{\text{MOF}}} \mathbf{v}_j \right] \quad (6)$$

$$J_{c2, \text{gas}} = \frac{1}{V} \left[h_{\text{gas}} \sum_{j=1}^{N_{\text{gas}}} \mathbf{v}_j \right] \quad (7)$$

$$J_v = \frac{1}{V} \left[\frac{1}{2} \sum_{i=1}^N \sum_{j=1, j \neq i}^N \mathbf{r}_{ij} (\mathbf{v}_j \cdot \mathbf{F}_{ij}) \right] \quad (8)$$

Here, N_{MOF} and N_{gas} represent the number of atoms composing HKUST-1 and those of Ar atoms, respectively. Furthermore, we calculated the thermal conductivity of each term shown in Eqs. (4)–(8) using the following formula [35].

$$k_\xi = \frac{V}{3k_B T^2} \int_0^\infty \langle J_\xi(t) \cdot J(0) \rangle dt \quad (9)$$

In Eq. (9), J_ξ represents a component of the instantaneous heat flux (Eqs. (4)–(8)), and k_ξ is the thermal conductivity calculated using J_ξ . In this study, we calculated the decomposed thermal conductivities $k_{c1, \text{MOF}}$, $k_{c1, \text{gas}}$, $k_{c2, \text{MOF}}$, $k_{c2, \text{gas}}$, and k_v for Ar-loaded HKUST-1. For pristine HKUST-1, we calculated $k_{c1, \text{MOF}}$ and k_v . The overall thermal conductivity k_{all} was obtained considering all the heat-flux terms in Eq. (2). Moreover, we defined k_{acc} as the cumulative sum of the thermal conductivities of all the components.

$$k_{\text{acc}} = k_{c1, \text{MOF}} + k_{c1, \text{gas}} - k_{c2, \text{MOF}} - k_{c2, \text{gas}} + k_v \quad (10)$$

Here, the subscripts of “c1, MOF” and “c1, gas” are the kinetic contributions that are mainly determined by the instantaneous energies of HKUST-1 and Ar, respectively. The subscripts of “c2, MOF” and “c2, gas” are the kinetic contributions that are mainly determined by the average partial enthalpies of HKUST-1 and Ar, respectively. The subscript of “v” is the contribution of the virial term.

Following previous studies, we introduced a cutoff time for performing the integrations shown in Eqs. (1) and (9). This is because the HCACF cannot be integrated over infinite time. In a previous study, Howell [33] calculated the root-mean-square of the heat current cross-correlation functions as

$$W = \sqrt{\frac{\langle S_x(t)S_y(0) \rangle^2 + \langle S_y(t)S_z(0) \rangle^2 + \langle S_z(t)S_x(0) \rangle^2}{3}} \quad (11)$$

and estimated the magnitude of the noise. Here, $S(t)$ is the heat current and $S_i(t) = VJ_i(t)$ ($i = x, y$, or z). The HCACF was truncated when W exceeded the HCACF, and the fitting curve of the HCACF up to the cutoff time was determined.

In another method, Chen et al. [34] defined a function $F(t)$ as shown below.

$$F(t) = \frac{|\sigma(t, t + \delta t)|}{|E(t, t + \delta t)|} \quad (12)$$

They determined the cutoff time as the time at which the magnitude of the function became greater than one. Here, $\sigma(t, t + \delta t)$ is the standard

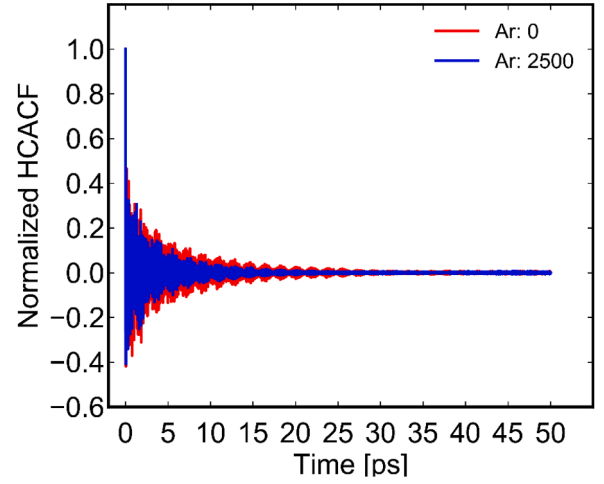


Fig. 2. Relationship between normalized HCACF and correlation time for pristine HKUST-1 (red line) and HKUST-1 loaded with 2500 Ar atoms (blue line).

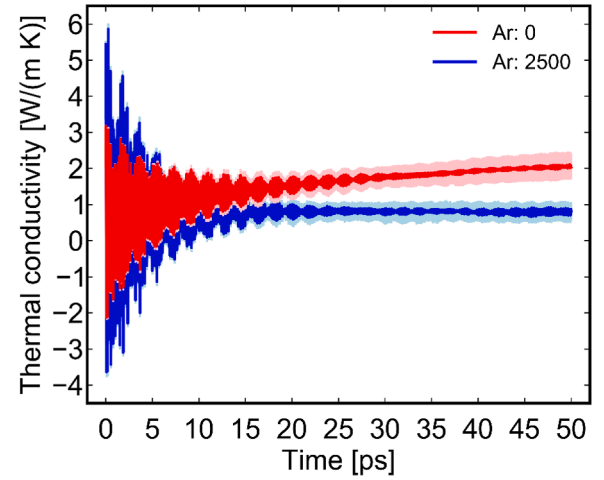


Fig. 3. Relationship between average thermal conductivity and correlation time with its standard deviation for pristine HKUST-1 (red line) and HKUST-1 loaded with 2500 Ar atoms (blue line).

deviation and $E(t, t + \delta t)$ is the expected value of the HCACF between the correlation times of t and $t + \delta t$.

In this study, we devised a new method for truncating the HCACF, wherein the cutoff time τ_c was defined as the correlation time when the fluctuations of the HCACF sufficiently converged. To quantify the fluctuation, we defined $D(t)$ as follows.

$$D(t) = \sigma(t, t + \delta t) \quad (13)$$

Here, σ denotes the standard deviation of the normalized HCACF between the correlation times of t and $t + \delta t$. Subsequently, we defined the cutoff time τ_c as the time required for the convergence of $D(t)$. We calculated the normalized HCACF as $\langle J(0) \cdot J(t) \rangle / \langle J(0) \cdot J(0) \rangle$.

3. Results and discussion

Figs. 2 and 3 show the average values of the normalized HCACF and thermal conductivity, respectively. The red lines in these figures show the values for pristine HKUST-1 while blue lines show the values for HKUST-1 loaded with 2500 Ar atoms. In Fig. 3, the pink and light-blue lines show the standard deviations of the values obtained over 10 simulations. As shown in Fig. 2, the HCACF for the pristine case converges at

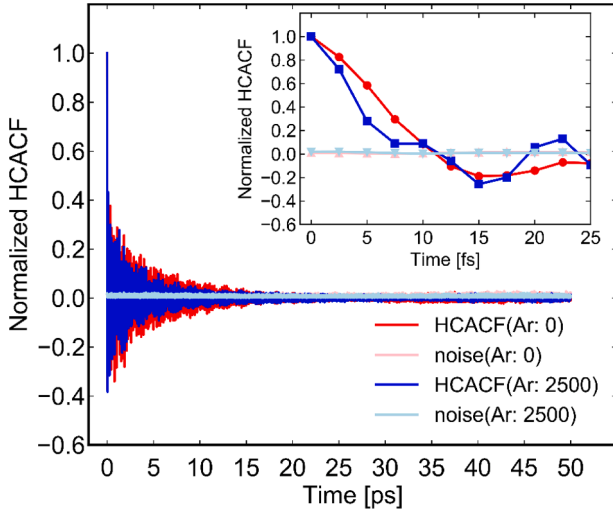


Fig. 4. Normalized HCACF and the noise function for pristine HKUST-1 (red line) and HKUST-1 loaded with 2500 Ar atoms (blue line). The inset is the enlarged views of normalized HCACF and the noise at small correlation time.

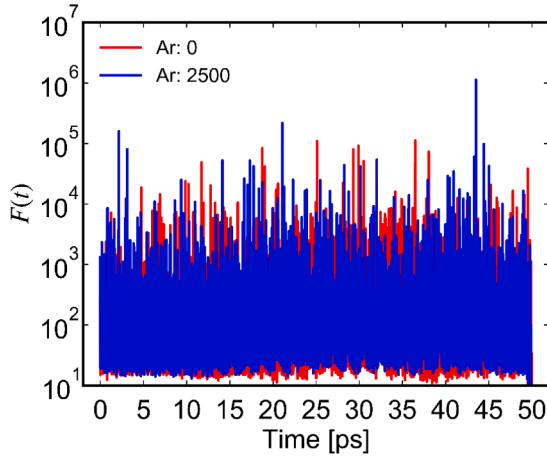


Fig. 5. Relative fluctuation of HCACF obtained by a single simulation run for pristine HKUST-1 (red line) and HKUST-1 loaded with 2500 Ar atoms (blue line).

about 30 ps, whereas the thermal conductivity (Fig. 3) increases slightly with correlation time. This implies that the HCACF does not perfectly fluctuate across a value of zero. For the HKUST-1 loaded with 2500 Ar atoms, the fluctuation in thermal conductivity is larger than that observed for the pristine case, and the thermal conductivity converges at about 25 ps. This convergence can be attributed to the shorter mean free path of phonons in the HKUST-1 loaded with Ar compared to that in the pristine case. In both cases, the cutoff time must be qualitatively determined for integrating the HCACFs.

First, we applied the method proposed by Howell [33] and defined \dot{W} (Eq. (14)).

$$\dot{W} = \frac{1}{\sqrt{2}} W \quad (14)$$

$$= \sqrt{\frac{\langle J_x(t)J_y(0) \rangle^2 + \langle J_y(t)J_z(0) \rangle^2 + \langle J_z(t)J_x(0) \rangle^2}{3}}$$

Here, W denotes the noise function defined in Eq. (11). Fig. 4 shows the normalized values of HCACF and \dot{W} for the pristine case and the system loaded with 2500 Ar atoms. The light-colored lines show the

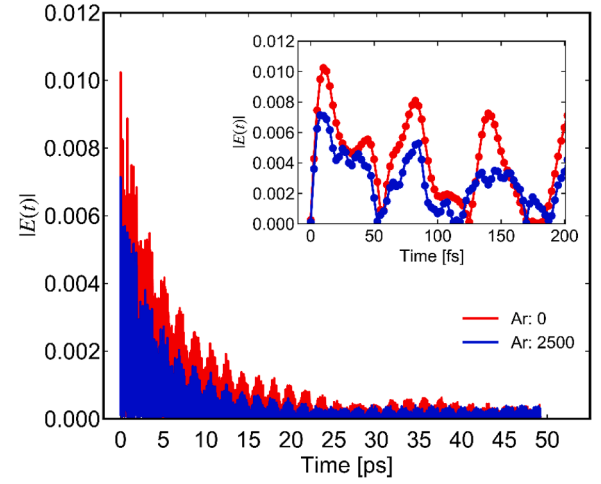


Fig. 6. Mean values of normalized HCACF in the time interval $(t, t+\delta)$ for pristine HKUST-1 (red line) and HKUST-1 loaded with 2500 Ar atoms (blue line). The insets are the enlarged views at small correlation time.

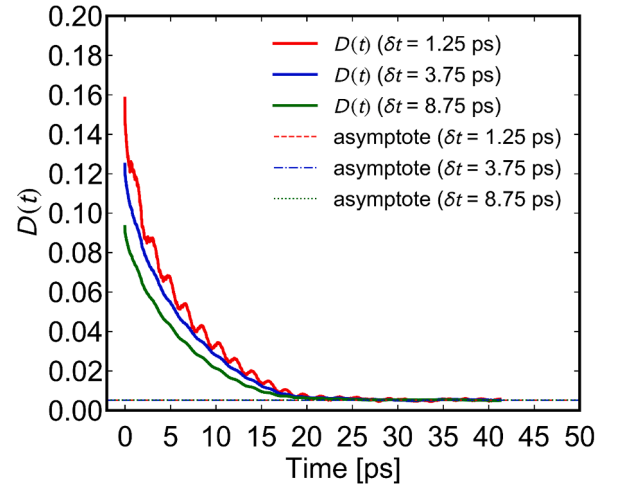


Fig. 7. $D(t)$ curve and their asymptotes ($\delta t = 1.25$ ps, 3.75 ps, and 8.75 ps).

values of the noise function \dot{W} . The cutoff time of the integration was determined as the correlation time when the noise exceeded the magnitude of HCACF. As shown in the insets of Fig. 4, the cutoff time in both cases is 0.0125 ps. This is the shortest correlation time corresponding to negative values of the HCACFs. Considering the typical HCACF fluctuations observed for MOFs, the cutoff time determined was too small, indicating that the method proposed by Howell is not suitable.

Next, we applied the method proposed by Chen et al. [34] and calculated $F(t)$ based on Eq. (12). Fig. 5 shows the $F(t)$ of pristine HKUST-1 and HKUST-1 loaded with 2500 Ar atoms. $F(t)$ fluctuates significantly, regardless of the correlation times. In addition, Fig. 6 shows the mean value of the normalized HCACF ($|E(t, t+\delta t)|$ in Eq. (12)) for pristine HKUST-1 and HKUST-1 loaded with 2500 Ar atoms. $|E(t, t+\delta t)|$ fluctuates significantly and as can be observed from the insets, $|E(t, t+\delta t)|$ assumes small values regardless of the range of correlation times. These small values lead to $F(t)$ spikes (Fig. 5). Therefore, the convergence of the HCACF cannot be defined using the function $F(t)$ given in Eq. (12).

In summary, the methods proposed by Howell and Chen et al. are not suitable for evaluating the HCACFs of the MOF. This is because the HCACFs of the MOF fluctuate across the zero value for all correlation times. It should be noted that using the methods proposed in the

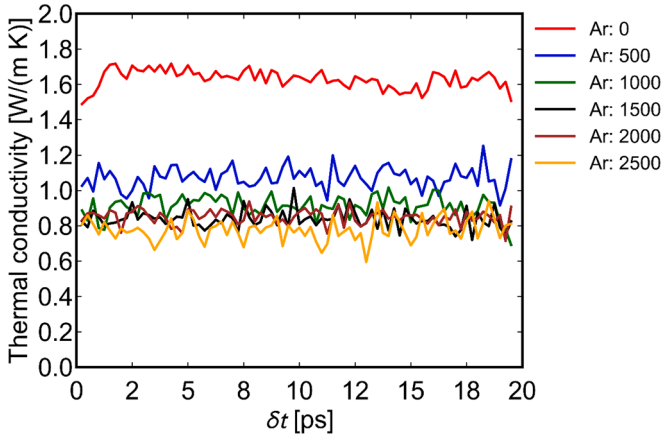


Fig. 8. Effect of time width δt on thermal conductivity.

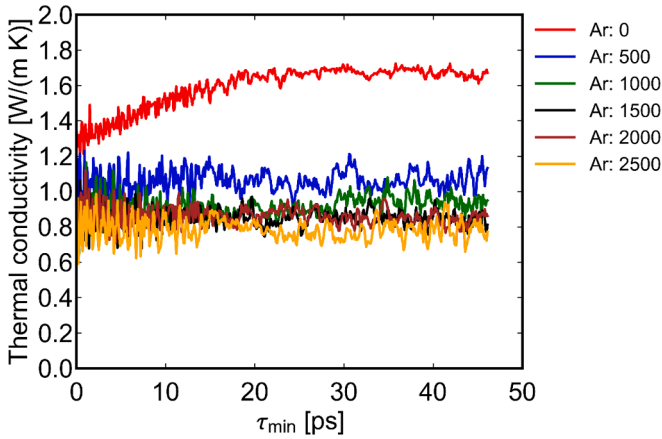
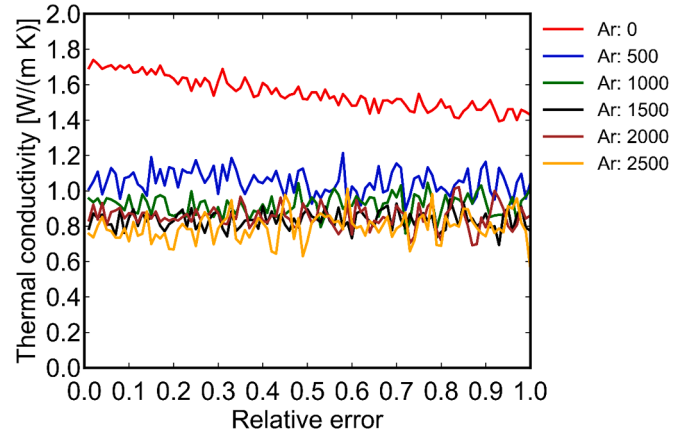


Fig. 9. Effect of τ_{\min} on thermal conductivity.

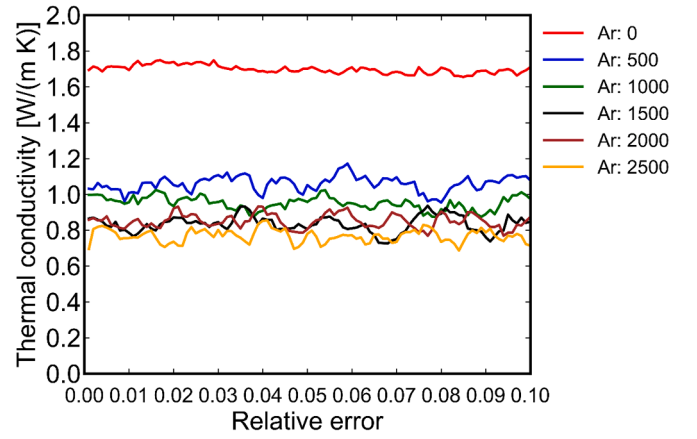
previous studies, the HCACFs were observed to fluctuate around positive values for small correlation times.

In this study, we devised a new method for truncating the HCACF. As shown in Fig. 3, the thermal conductivity of pristine HKUST-1 increases slightly with correlation time although the HCACF (Fig. 2) converges. Considering the limited amplitude of fluctuations in the HCACF for long correlation times, the phonon modes may not contribute significantly to the observed increase within the correlation time. Therefore, we determined the cutoff time based on the convergence of the HCACF fluctuations. To quantify the fluctuation, we defined $D(t)$ as $D(t) = \sigma(t, t + \delta t)$, where σ is the standard deviation of the normalized HCACF between the correlation times of t and $t + \delta t$ (Eq. (13)). Fig. 7 shows the curves of $D(t)$ for the pristine case for three different values of δt : 1.25 ps, 3.75 ps, and 8.75 ps. The value of the asymptote was determined from the mean value of the $D(t)$ in the correlation time between τ_{\min} and τ_{\max} , where τ_{\max} is 50 ps in this study. Subsequently, to determine the convergence of the $D(t)$, we defined the threshold value of the relative errors from the asymptote. $D(t)$ was considered to converge when the relative error of the $D(t)$ from the asymptote was smaller than the threshold value. We defined the cutoff time τ_c as the time required for $D(t)$ to converge. In summary, three parameters were defined to determine the cutoff time: the time width δt , τ_{\min} to determine the asymptote, and the threshold of error from the asymptote.

To confirm that the parameters did not significantly affect the results, we evaluated the overall thermal conductivity varying one parameter and keeping the values of the other parameters fixed. First, we varied the time width δt (a parameter involved in $D(t)$ calculations), with the threshold value and τ_{\min} fixed at 0.1 and 30 ps, respectively.



(a) Relative error (< 1.0).



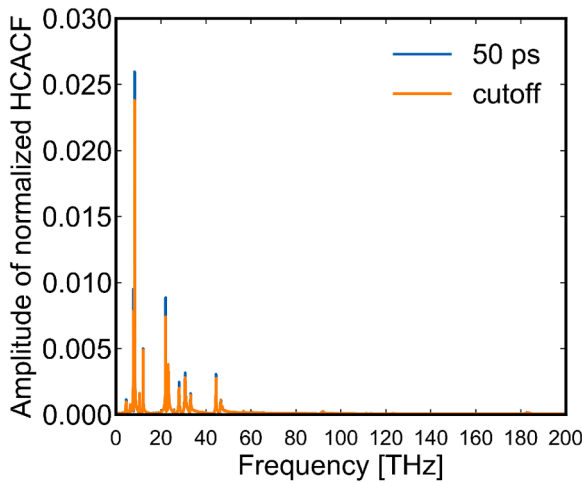
(b) Relative error (< 0.1).

Fig. 10. Effect of threshold value on thermal conductivity.

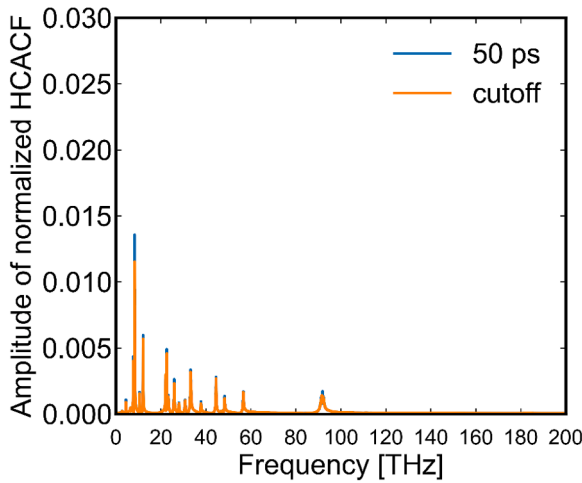
Fig. 8 shows the relationship between the value of δt and thermal conductivity. The results indicate that δt does not significantly affect the value of thermal conductivity. However, the result of the $D(t)$ curves in Fig. 7 shows that the fluctuations of $D(t)$ become more pronounced at $\delta t = 1.25$ ps, making it difficult to determine the convergence time. At $\delta t = 8.75$ ps, $D(t)$ declines without fluctuations. In addition, $D(t)$ is calculated between t and $t + \delta t$ and the HCACF is calculated until a correlation time of 50 ps. This implies that the $D(t)$ can be calculated up to $D(50 - \delta t)$ and the amount of data required to calculate the asymptote decreases as the value of δt increases. Hence, too large values of δt lead to unreliable values of the asymptote, while too small values of δt complicate an accurate determination of the convergence time.

Next, we varied the value of τ_{\min} , fixing δt and the threshold error at 3.75 ps and 0.1, respectively. τ_{\min} is a parameter used to determine the asymptote of $D(t)$. Fig. 9 shows the thermal conductivities with respect to τ_{\min} . The thermal conductivity of the pristine case increases slightly until a τ_{\min} of 25 ps. As evident from Fig. 7, too small values of τ_{\min} can lead to invalid results, because the value of the asymptote can be inconsistent with the convergence value of the $D(t)$.

Finally, we investigated the influence of the threshold value of the relative error on the results based on the calculated $D(t)$ and its asymptote. Fig. 10 shows the relationship between the thermal conductivity and the threshold value for δt and τ_{\min} of 3.75 ps and 30 ps, respectively. Fig. 10 (a) and 10 (b) show the thermal conductivities corresponding to a maximum relative error of 1.0 and 0.1, respectively. These figures indicate that the thermal conductivity does not change significantly when the relative error is less than 0.1. Based on the above



(a) Pristine HKUST-1.



(b) HKUST-1 loading 2500 Ar atoms.

Fig. 11. The Fourier transform of normalized HCACF.

investigation, we determined the time width δt , the threshold of error, and τ_{\min} as 3.75 ps, 0.1, and 30 ps, respectively. The pristine and the Ar-loaded HKUST-1 systems (Figs. 8–10) exhibited different results, which can be attributed to the trends of the HCACFs. Compared to the Ar-loaded HKUST-1, the pristine HKUST-1 exhibited smaller amplitudes of thermal-conductivity fluctuations (Fig. 3). However, the thermal conductivity of the Ar-loaded HKUST-1 converged relatively well. Similar trends are observed in Figs. 8–10.

Furthermore, we considered the fluctuation in the HCACF and investigated their frequency characteristics. For this, we obtained the Fourier transform of the normalized HCACF [25,41] and compared the modes before and after applying the truncation method proposed in this study. In previous studies, the Fourier transform of HCACF was calculated to investigate the modes contributing to the thermal conductivity. Therefore, HCACF must include these modes even after truncating HCACF for finite integration in the Green–Kubo formula.

When the truncation method was not applied, the HCACFs were integrated for 50 ps. Fig. 11 (a) and 11 (b) show examples of the result obtained for pristine HKUST-1 and HKUST-1 loaded with 2500 Ar atoms, respectively. The blue lines show the results obtained when the HCACF was integrated to 50 ps, and the orange lines show those obtained when the integration was performed till the cutoff time determined by the truncation method. The figures reveal that the positions of

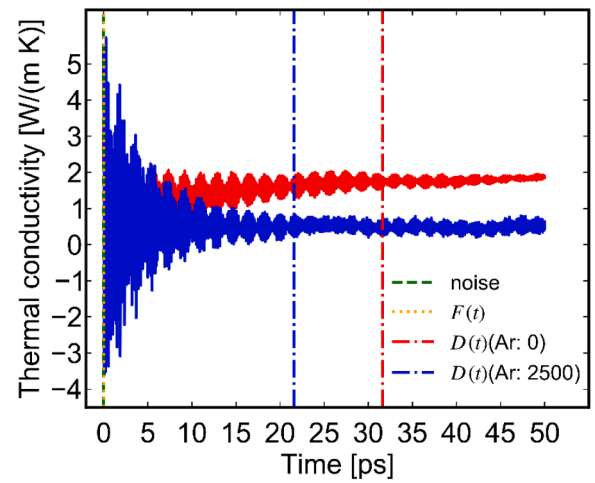
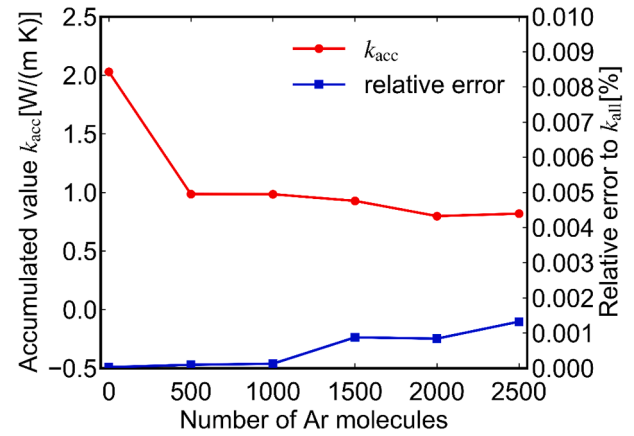


Fig. 12. Example of the determined cutoff time for pristine HKUST-1 (red line) and HKUST-1 loaded with 2500 Ar atoms (blue line).

Fig. 13. Values of k_{acc} and the relative errors to k_{all} .

the peaks do not change significantly, suggesting that our method efficiently incorporates the contributions of the dominant phonon modes to the thermal conductivities. This result confirms the validity of the proposed truncation method. The Fourier-transformed HCACFs were obtained in one simulation run, but did not change significantly depending on each run.

Fig. 12 shows the relationship between the thermal conductivity and correlation time obtained by a single simulation run. Each vertical line shows the cutoff time determined by each method (green line: method by Howell; orange line: method by Chen et al.; red and blue lines: method proposed in this study). As mentioned above, the cutoff time determined using the method from Howell was 0.0125 ps. The cutoff time determined by applying $F(t)$ was 0.0 ps in all cases because the magnitude of $F(t)$ was much larger than 1.0 as shown in Fig. 5. When $D(t)$ was applied, the determined time τ_c varied in each simulation run; however, the range of τ_c was 15–35 ps in all cases.

Previous studies have focused on the overall thermal conductivities of MOFs. In this study, we investigated the thermal conductivity in more detail by dividing it into its constituent components and then calculating the values of each component ($J_{\text{c1,MOF}}$, $J_{\text{c1,gas}}$, $J_{\text{c2,MOF}}$, $J_{\text{c2,gas}}$, and J_v). To confirm the validation of the method in accurately evaluating the contributions of each component, the accumulated thermal conductivity k_{acc} was compared with the overall value k_{all} . The k_{acc} can be obtained by Eqs. (4)–(10) while the k_{all} can be obtained based on Eqs. (1) and (2).

Fig. 13 shows the value of k_{acc} and the relative error of k_{acc} from the value of k_{all} with respect to the number of Ar atoms loaded in HKUST-1.

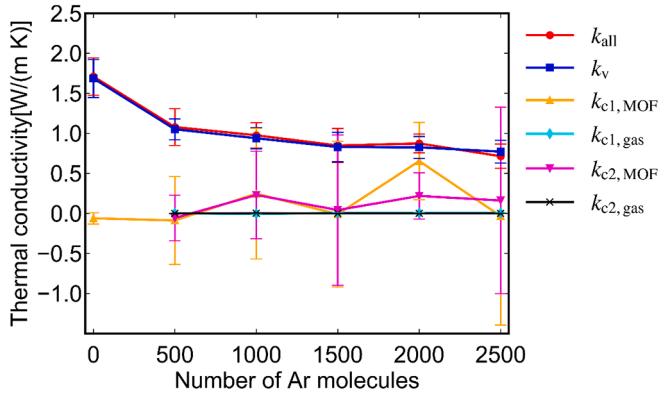


Fig. 14. Decomposed thermal conductivities.

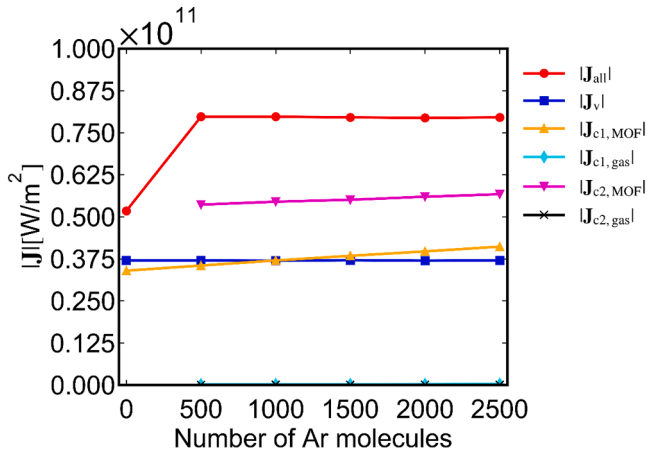


Fig. 15. Time-average values of the absolute heat fluxes.

The values of k_{acc} are well-consistent with the values of k_{all} for all cases, indicating we can validate the decomposition of thermal conductivity.

Fig. 14 shows the relationship between the number of the loaded Ar atoms and decomposed thermal conductivities after applying the cutoff time τ_c defined in this study. The HCACF was truncated for each component in each simulation run. As can be observed from the figure, the overall thermal conductivity of the Ar-loaded HKUST-1 is lower than that of the pristine case in all cases. This trend was observed in previous studies for other fluid molecules, and it can be attributed to the phonon scatterings [23,24,28]. A smaller k_{all} is observed when the number of Ar atoms is 2500, compared to when the number is 500. This is because of the increased frequency of interactions between the Ar atoms and atoms composing HKUST-1 as the number of Ar atoms loaded increases. The values of k_v demonstrate that the interaction of the atoms impacts the thermal transport in the system more significantly than the microscopic convection of the atoms. In addition, the values of $k_{c1, MOF}$ and $k_{c2, MOF}$ basically exhibit similar values (Fig. 14), resulting in the mutual cancellation of their most contributions. Notably, they largely varied depending on the number of Ar atoms. Eq. (9) suggests that the magnitudes of the heat fluxes $J_{c1, MOF}$ and $J_{c2, MOF}$, and their correlations with $J(0)$ may influence the behaviors of $k_{c1, MOF}$ and $k_{c2, MOF}$. Fig. 15 shows the time-averaged values of the absolute instantaneous heat flux. The trends of $|J_{c1, MOF}|$ and $|J_{c2, MOF}|$ are not consistent with those of

$k_{c1, MOF}$ and $k_{c2, MOF}$. This implies that $k_{c1, MOF}$ and $k_{c2, MOF}$ are independent of the magnitude of the heat flux. Hence, the correlation of $J_{c1, MOF}$ and $J_{c2, MOF}$ with $J(0)$ may determine the values. Focusing on the values of $k_{c1, gas}$ and $k_{c2, gas}$, they are much smaller than those of other components. This can be attributed to the difference in the number of atoms; HKUST-1 consists of 16846 atoms with a maximum of 2500 Ar atoms. As shown in Fig. 14, the time-averaged values of $k_{c1, MOF}$, $k_{c2, MOF}$, $k_{c1, gas}$, and $k_{c2, gas}$ are negative in some cases. To understand more details, Table 1 lists the $k_{c1, MOF}$ of the pristine HKUST-1 for each simulation run. Table 2 lists the $k_{c1, MOF}$, $k_{c2, MOF}$, $k_{c1, gas}$, and $k_{c2, gas}$ of HKUST-1 loaded with 2500 Ar atoms for each simulation run. The values obtained in one simulation run are either negative or positive, highlighting the ambiguity presented when calculating the thermal conductivity of MOFs through EMD simulations. The size effect of the system can lead to the negative thermal conductivity components. However, the computational cost is limited, and the size of the system was sufficient to calculate the thermal conductivity based on a previous study [26]. We note that the contributions of $k_{c1, MOF}$, $k_{c2, MOF}$, $k_{c1, gas}$, and $k_{c2, gas}$ are much smaller than that of k_v , as the contributions of $k_{c1, MOF}$ and $k_{c2, MOF}$ cancel each other out, similar to those of $k_{c1, gas}$ and $k_{c2, gas}$.

4. Conclusions

In this study, we performed EMD simulations and investigated the thermal transport properties of HKUST-1 loaded with Ar atoms, and examined methods to truncate HCACF to obtain the thermal conductivity of the MOF more accurately using the Green-Kubo formula. The results revealed that it was difficult to apply the conventional methods used in previous studies to determine the cutoff time for integrating HCACF because the methods were not suitable for the profile of the MOF HCACFs. Therefore, we devised a new method for truncating MOF HCACFs and confirmed that the parameters used in our method do not significantly affect the results. The obtained thermal conductivity was decomposed into its constituent components and the contributions of each term in the instantaneous heat flux were evaluated. The thermal conductivity was observed to decrease when Ar atoms were loaded. In addition, the virial term in the heat flux was dominant over the thermal conductivity despite the increase in the number of loaded Ar atoms. This indicated that, compared to the kinetic contribution, the interaction of the atoms had a more significant effect on the thermal conductivity. However, the decomposed thermal conductivities induced an ambiguity while calculating the thermal conductivities of MOFs through EMD simulations. Finally, the proposed method is useful for generally treating the truncation of HCACFs and determining the thermal conductivity of complex materials such as MOFs.

Funding

This research did not receive any specific grant from funding agencies in the public, commercial, or not-for-profit sectors.

CRediT authorship contribution statement

Hideaki Ito: Writing – original draft, Visualization, Validation, Software, Methodology, Investigation, Formal analysis, Data curation, Conceptualization. **Kunio Fujiwara:** Writing – review & editing, Supervision, Resources, Project administration, Conceptualization. **Masahiko Shibahara:** Writing – review & editing, Supervision, Resources.

Table 1

Values of $k_{c1, MOF}$ of the pristine HKUST-1 for each simulation run.

case	1	2	3	4	5	6	7	8	9	10
$k_{c1, MOF}$	3.85×10^{-2}	-9.59×10^{-2}	-4.96×10^{-2}	1.44×10^{-2}	-5.89×10^{-2}	-0.107	-7.56×10^{-3}	-0.191	-1.21×10^{-2}	-0.150

Table 2Values of $k_{c1, \text{MOF}}$, $k_{c2, \text{MOF}}$, $k_{c1, \text{gas}}$, and $k_{c2, \text{gas}}$ of HKUST-1 loading 2500 Ar atoms for each simulation run.

case	1	2	3	4	5	6	7	8	9	10
$k_{c1, \text{MOF}}$	-0.235	3.70	-0.709	0.504	-0.304	-1.53	-0.757	0.199	-0.205	-0.999
$k_{c2, \text{MOF}}$	0.340	3.29	-0.757	0.463	-0.468	-0.673	-0.162	0.644	-8.05×10^{-2}	-0.989
$k_{c1, \text{gas}}$	2.88×10^{-3}	5.84×10^{-3}	6.61×10^{-3}	4.55×10^{-3}	6.68×10^{-3}	6.53×10^{-4}	7.48×10^{-3}	4.64×10^{-3}	5.63×10^{-3}	6.23×10^{-3}
$k_{c2, \text{gas}}$	-6.59×10^{-4}	2.74×10^{-3}	-3.81×10^{-4}	2.17×10^{-4}	-1.28×10^{-3}	5.91×10^{-4}	-7.98×10^{-4}	-3.76×10^{-4}	3.02×10^{-4}	-1.19×10^{-3}

Declaration of competing interest

The authors declare that they have no known competing financial interests or personal relationships that could have appeared to influence the work reported in this paper.

Data availability

Data will be made available on request.

References

- [1] D. Tanaka, M. Higuchi, S. Horike, R. Matsuda, Y. Kinoshita, N. Yanai, S. Kitagawa, Storage and sorption properties of acetylene in jungle-gym-like open frameworks, *Chem. Asian J.* 3 (2008), <https://doi.org/10.1002/asia.200800112>.
- [2] O.K. Farha, A.O. Yazaydin, I. Eryazici, C.D. Malliakas, B.G. Hauser, M. G. Kanatzidis, S.T. Nguyen, R.Q. Snurr, J.T. Hupp, De novo synthesis of a metal-organic framework material featuring ultrahigh surface area and gas storage capacities, *Nat. Chem.* 2 (2010), <https://doi.org/10.1038/nchem.834>.
- [3] M. Xue, Y. Liu, R.M. Schaffino, S. Xiang, X. Zhao, G.S. Zhu, S.L. Qiu, B. Chen, New prototype isoreticular metal-organic framework Zn 4O(FMA) 3 for gas storage, *Inorg. Chem.* 48 (2009), <https://doi.org/10.1021/ic900486r>.
- [4] D.A. Reed, B.K. Keitz, J. Oktawiec, J.A. Mason, T. Runcevski, D.J. Xiao, L. E. Darago, V. Crocellà, S. Bordiga, J.R. Long, A spin transition mechanism for cooperative adsorption in metal-organic frameworks, *Nature* 550 (2017), <https://doi.org/10.1038/nature23674>.
- [5] S. Yang, J. Sun, A.J. Ramirez-Cuesta, S.K. Callear, W.I.F. David, D.P. Anderson, R. Newby, A.J. Blake, J.E. Parker, C.C. Tang, M. Schröder, Selectivity and direct visualization of carbon dioxide and sulfur dioxide in a decorated porous host, *Nat. Chem.* 4 (2012), <https://doi.org/10.1038/nchem.1457>.
- [6] J. Li, X. Han, X. Zhang, A.M. Sheveleva, Y. Cheng, F. Tuna, E.J.L. McInnes, L. J. McCormick McPherson, S.J. Teat, L.L. Daemen, A.J. Ramirez-Cuesta, M. Schröder, S. Yang, Capture of nitrogen dioxide and conversion to nitric acid in a porous metal-organic framework, *Nat. Chem.* 11 (2019), <https://doi.org/10.1038/s41557-019-0356-0>.
- [7] Y. Khabzina, J. Dhainaut, M. Ahlhelm, H.J. Richter, H. Reinsch, N. Stock, D. Farrusseng, Synthesis and shaping scale-up study of functionalized UiO-66 MOF for ammonia air purification filters, *Ind. Eng. Chem. Res.* 57 (2018), <https://doi.org/10.1021/acs.iecr.8b00808>.
- [8] E.D. Bloch, W.L. Queen, R. Krishna, J.M. Zadrozny, C.M. Brown, J.R. Long, Hydrocarbon separations in a metal-organic framework with open iron(II) coordination sites, *Science* 335 (2012), <https://doi.org/10.1126/science.1217544>.
- [9] J.R. Li, R.J. Kuppler, H.C. Zhou, Selective gas adsorption and separation in metal-organic frameworks, *Chem. Soc. Rev.* 38 (2009), <https://doi.org/10.1039/b802426j>.
- [10] G.L. Smith, J.E. Eyley, X. Han, X. Zhang, J. Li, N.M. Jacques, H.G.W. Godfrey, S. P. Argent, L.J. McCormick McPherson, S.J. Teat, Y. Cheng, M.D. Frogley, G. Cinque, S.J. Day, C.C. Tang, T.L. Easun, S. Rudić, A.J. Ramirez-Cuesta, S. Yang, M. Schröder, Reversible coordinative binding and separation of sulfur dioxide in a robust metal-organic framework with open copper sites, *Nat. Mater.* 18 (2019), <https://doi.org/10.1038/s41563-019-0495-0>.
- [11] G. Lu, J.T. Hupp, Metal-organic frameworks as sensors: a ZIF-8 based fabry-pérot device as a selective sensor for chemical vapors and gases, *J. Am. Chem. Soc.* 132 (2010), <https://doi.org/10.1021/ja101415b>.
- [12] M. Schulz, A. Gehl, J. Schlenkrich, H.A. Schulze, S. Zimmermann, A. Schaate, A calixarene-based metal-organic framework for highly selective NO₂ detection, *Angew. Chem. Int. Ed.* 57 (2018), <https://doi.org/10.1002/anie.201805355>.
- [13] L.E. Kreno, K. Leong, O.K. Farha, M. Allendorf, R.P. Van Duyne, J.T. Hupp, Metal-organic framework materials as chemical sensors, *Chem. Rev.* 112 (2012), <https://doi.org/10.1021/cr200324t>.
- [14] S. Horike, M. Dincă, K. Tamaki, J.R. Long, Size-selective Lewis acid catalysis in a microporous metal-organic framework with exposed Mn²⁺ coordination sites, *J. Am. Chem. Soc.* 130 (2008), <https://doi.org/10.1021/ja800669j>.
- [15] C. De Wu, A. Hu, L. Zhang, W. Lin, A homochiral porous metal-organic framework for highly enantioselective heterogeneous asymmetric catalysis, *J. Am. Chem. Soc.* 127 (2005), <https://doi.org/10.1021/ja052431t>.
- [16] A. Bavykina, N. Kolobov, I.S. Khan, J.A. Bau, A. Ramirez, J. Gascon, Metal-organic frameworks in heterogeneous catalysis: recent progress, new trends, and future perspectives, *Chem. Rev.* 120 (2020), <https://doi.org/10.1021/acs.chemrev.9b00685>.
- [17] M. Giménez-Marqués, A. Santiago-Portillo, S. Navalón, M. Álvaro, V. Briois, F. Nouar, H. Garcia, C. Serre, Exploring the catalytic performance of a series of bimetallic MIL-100(Fe, Ni) MOFs, *J. Mater. Chem. A* 7 (2019), <https://doi.org/10.1039/c9ta01948k>.
- [18] J. Lee, O.K. Farha, J. Roberts, K.A. Scheidt, S.T. Nguyen, J.T. Hupp, Metal-organic framework materials as catalysts, *Chem. Soc. Rev.* 38 (2009), <https://doi.org/10.1039/b807080f>.
- [19] Y.H. Hu, L. Zhang, Hydrogen storage in metal-organic frameworks, *Adv. Mater.* 22 (2010), <https://doi.org/10.1002/adma.200902096>.
- [20] J. Ren, H.W. Langmi, B.C. North, M. Mathe, Review on processing of metal-organic framework (MOF) materials towards system integration for hydrogen storage, *Int. J. Energy. Res.* 39 (2015), <https://doi.org/10.1002/er.3255>.
- [21] M. Ding, R.W. Flaig, H.L. Jiang, O.M. Yaghi, Carbon capture and conversion using metal-organic frameworks and MOF-based materials, *Chem. Soc. Rev.* 48 (2019), <https://doi.org/10.1039/c8cs00829a>.
- [22] C. Chen, Y.R. Lee, W.S. Ahn, CO₂ adsorption over metal-organic frameworks: a mini review, *J. Nanosci. Nanotechnol.* 16 (2016), <https://doi.org/10.1166/jnn.2016.10971>.
- [23] H. Fan, C. Yang, Y. Zhou, Ultralong mean free path phonons in HKUST-1 and their scattering by water adsorbates, *Phys. Rev. B* 106 (2022), <https://doi.org/10.1103/PhysRevB.106.085417>.
- [24] H. Babaei, C.E. Wilmer, Mechanisms of heat transfer in porous crystals containing adsorbed gases: applications to metal-organic frameworks, *Phys. Rev. Lett.* 116 (2016), <https://doi.org/10.1103/PhysRevLett.116.025902>.
- [25] X. Zhang, J. Jiang, Thermal conductivity of zeolitic imidazolate framework-8: a molecular simulation study, *J. Phys. Chem. C* 117 (2013), <https://doi.org/10.1021/jp405156y>.
- [26] M. Islamov, H. Babaei, C.E. Wilmer, Influence of missing linker defects on the thermal conductivity of metal-organic framework HKUST-1, *ACS Appl. Mater. Interfaces* 12 (2020), <https://doi.org/10.1021/acsami.0c16127>.
- [27] H. Babaei, A.J.H. McGaughey, C.E. Wilmer, Transient mass and thermal transport during methane adsorption into the metal-organic framework HKUST-1, *ACS Appl. Mater. Interfaces* 10 (2018), <https://doi.org/10.1021/acsami.7b13605>.
- [28] H. Babaei, M.E. DeCoster, M. Jeong, Z.M. Hassan, T. Islamoglu, H. Baumgart, A.J. H. McGaughey, E. Redel, O.K. Farha, P.E. Hopkins, J.A. Malen, C.E. Wilmer, Observation of reduced thermal conductivity in a metal-organic framework due to the presence of adsorbates, *Nat. Commun.* 11 (2020), <https://doi.org/10.1038/s41467-020-17822-0>.
- [29] J. Hu, C. Liu, Q. Li, X. Shi, Molecular simulation of thermal energy storage of mixed CO₂/IRMOF-1 nanoparticle nanofluid, *Int. J. Heat Mass Transf.* 125 (2018), <https://doi.org/10.1016/j.ijheatmasstransfer.2018.04.162>.
- [30] B.L. Huang, A.J.H. McGaughey, M. Kaviani, Thermal conductivity of metal-organic framework 5 (MOF-5): Part I. Molecular dynamics simulations, *Int. J. Heat Mass Transf.* 50 (2007), <https://doi.org/10.1016/j.ijheatmasstransfer.2006.10.002>.
- [31] R. Kubo, Statistical-mechanical theory of irreversible processes. I. General theory and simple applications to magnetic and conduction problems, *J. Phys. Soc. Jpn.* 12 (1957), <https://doi.org/10.1143/JPSJ.12.570>.
- [32] M.S. Green, Markoff random processes and the statistical mechanics of time-dependent phenomena. II. Irreversible processes in fluids, *J. Chem. Phys.* 22 (1954), <https://doi.org/10.1063/1.1740082>.
- [33] P.C. Howell, Comparison of molecular dynamics methods and interatomic potentials for calculating the thermal conductivity of silicon, *J. Chem. Phys.* 137 (2012), <https://doi.org/10.1063/1.4767516>.
- [34] J. Chen, G. Zhang, B. Li, How to improve the accuracy of equilibrium molecular dynamics for computation of thermal conductivity? *Phys. Lett. A* 374 (2010), <https://doi.org/10.1016/j.physleta.2010.03.067>.
- [35] H. Matsubara, G. Kikugawa, M. Ishikiriya, S. Yamashita, T. Ohara, Equivalence of the EMD- and NEMD-based decomposition of thermal conductivity into microscopic building blocks, *J. Chem. Phys.* 147 (2017), <https://doi.org/10.1063/1.4990593>.
- [36] L. Zhao, Q. Yang, Q. Ma, C. Zhong, J. Mi, D. Liu, A force field for dynamic Cu-BTC metal-organic framework, *J. Mol. Model.* 17 (2011), <https://doi.org/10.1007/s00894-010-0720-x>.
- [37] A.K. Rappé, C.J. Casewit, K.S. Colwell, W.A. Goddard, W.M. Skiff, UFF, a full periodic table force field for molecular mechanics and molecular dynamics simulations, *J. Am. Chem. Soc.* 114 (1992), <https://doi.org/10.1021/ja00051a040>.
- [38] S. Plimpton, Fast parallel algorithms for short-range molecular dynamics, *J. Comput. Phys.* 117 (1995), <https://doi.org/10.1006/jcph.1995.1039>.

- [39] H. Babaei, P. Keblinski, J.M. Khodadadi, Equilibrium molecular dynamics determination of thermal conductivity for multi-component systems, *J. Appl. Phys.* 112 (2012), <https://doi.org/10.1063/1.4749265>.
- [40] P. Boone, H. Babaei, C.E. Wilmer, Heat flux for many-body interactions: corrections to LAMMPS, *J. Chem. Theory Comput.* 15 (2019), <https://doi.org/10.1021/acs.jctc.9b00252>.
- [41] S.S. Sørensen, H. Johra, J.C. Mauro, M. Bauchy, M.M. Smedskjaer, Boron anomaly in the thermal conductivity of lithium borate glasses, *Phys. Rev. Mater.* 3 (2019), <https://doi.org/10.1103/PhysRevMaterials.3.075601>.